Coded QAM Backscatter Modulation for RFID

Colby Boyer, *Student Member IEEE*, and Sumit Roy, *Fellow IEEE*

***Abstract*—Radio Frequency Identification (RFID) systems, presently standardized under EPC Global Class-1 Gen-2, have attracted increasing interest as the next-generation technology for tagged object identification. One of the important objectives of this work is to highlight the fact that the performance of the backscatter uplink (determined by constellation choice and forward error correction) is coupled to the downlink via the power harvesting functionality. The concept of *normalized power loss per bit* is introduced for such RFID communication systems to capture the consequent trade-offs, that form the crux of the results. We explore the use of higher dimensional (4-QAM) modulation schemes in future RFID systems (beyond current binary modulation in Class-1 Gen 2) as a means to improve uplink bit rate. However, this results in significantly increased normalized power loss vis-a-vis 2-PSK, suggesting a role for FEC coding. New coded modulation schemes - based on unequal error protection - are proposed that provides additional degrees of freedom (via choice of code parameters) to trade-off spectral efficiency with normalized power loss. This is explored and quantified, resulting in design recommendations.**

***Index Terms*—Radiofrequency identification, modulation, coding, backscatter communication, EPC Class 1 Gen 2 Protocols.**

I. Introduction

RADIO Frequency Identification (RFID) technology seeks to replace present-day optical scanning of objects tagged with bar-codes so as to improve reliability and speed of item identification, as well as enabling additional features such as enhanced inventory management. The promise of RFID and its eventual widespread successful deployment within a commercial supply chain is predicated on low cost, passive tags that support reliable, fast reading of tag IDs by readers. However, these two simultaneous objectives (ultra-cheap tags and a reliable, efficient system) are at odds due to extreme limitations on tag capabilities. This includes very limited memory and on-tag data processing, and (most relevant for our purposes), seriously constrained power availability[1]. Accordingly, RFID tag designs are being continually improved on various fronts - via improved circuitry and energy management approaches, among others.

An example of RFID tag re-engineering conformal to our vision of sensing applications [1] is represented by the Wireless Identification and Sensing Platform (WISP) [2]. A sensor network using RFID components would, first and foremost, require integration of sensors that in turn, incurs significant new energy cost. Second, the sensor data is expected to be transferred to a central repository, requiring enhanced uplink rates and reliability compared to present-day application of (one-time) reading of the EPC code.

Presently, poor tag sensitivity and power harvesting in passive tags limit the downlink range [3] and achievable link throughput. On the other hand, semi-passive tags which incorporate some energy storage mechanism but still use passive backscatter, are typically uplink limited. Hence uplink improvements (enhanced front-ends for power harvesting, circuit designs with lower sensitivity and more energy aware protocol stack) will be key to future RFID systems, as was explored in [3]. In this work, we continue to further explore different facets of the uplink-downlink coupling that relates achievable uplink rate/reliability with downlink power harvesting.

In its essential form, a passive RFID tag consists of a digital logic integrated circuit (IC), an antenna, and mixed-signal circuitry (possibly integrated into the IC) [4]. During uplink and downlink communication, the reader's radio frequency (RF) carrier wave energizes the RFID tag via power harvesting. Uplink communication occurs by modulating the antenna loading (via switching of a on-chip variable impedance) [5]. Such passive *backscatter modulation* obviates the need for the active components found in heterodyne systems, hence providing for low-cost tags but requiring power harvesting.

By choosing from a set of impedance loadings, the tag can map a sequence of digital symbols onto the backscattered waveforms. The current industry standard - EPC Global Gen-2 [6]- specifies two binary encoding schemes, FM0 and Miller sub-band coding, for the uplink, implemented with either two state amplitude shift keying (ASK) or phase shift keying (PSK). Both schemes use bi-orthogonal symbols for transmission and incorporate encoder memory in mapping past information bits onto current transmitted waveform. This suggests the benefits of maximum likelihood sequence estimation (MLSE) at the reader; however, it was shown in [7] that a linear receiver for FM0 operating over two successive symbols achieves near-MLSE performance.

It has recently been shown by [8] that it is feasible to build backscatter systems supporting higher order constellations, e.g. 4-QAM or 8-QAM. This opens up the possibility for coded modulation or other advanced modulation and coding combinations for passive backscatter RFID systems. However, improved spectral efficiency implies an energy cost. During nominal (non-backscatter) operation, the tag IC equivalent impedance is set to allow for maximum power transfer from the antenna. During backscatter modulation the tag's impedance is intentionally mismatched, and hence the power

Paper approved by E. Perrins, the Editor for Modulation Theory of the IEEE Communications Society. Manuscript received May 19, 2011; revised November 22, 2011 and January 18, 2012.

C. Boyer (corresponding author) and S. Roy are with the Department of Electrical Engineering at the University of Washington, Seattle 98195, WA (e-mail: {csboyer, sroy}@u.washington.edu).

This work was supported in part by the National Science Foundation under grant ECS 0824265.

Digital Object Identifier 10.1109/TCOMM.2012.051012.110317

[1]Passive tags have no separate battery source and must rely entirely on harvested energy.

harvested is reduced (compared to quiescent state).

Denote the power harvested under conjugate matched conditions as P_{match}, the average power harvested during backscatter as P_{avg}, and information bits per symbol (C). We introduce the metric, the *normalized power loss per information bit*

$$P_{loss} = \frac{P_{match} - P_{avg}}{C\, P_{match}} \quad (1)$$

Our objective in this work is two-fold: to a) investigate ways to improve uplink spectral efficiency and b) to characterize the associated normalized power loss per bit. Increasing the constellation order from binary signaling to 4-QAM doubles the spectral efficiency, but causes further power loss per bit. Our work investigates how the co-design of the 4-QAM constellation geometry and forward error correction (FEC) may be used to balance the normalized power loss per bit and increased spectral efficiency. We first establish an equivalent circuit model in Sec. II for the RFID tag in terms of a backscatter modulation design parameter that determines the trade-off between backscattered signal to the reader and the available power transferred to the tag. In Sec. III and Sec. IV, we explore uncoded 4-QAM constellation design such that the power loss during backscatter is minimized. Next in Sec. V, we investigate FEC encoding schemes suitable for 4-QAM modulation - these include traditional equal error protection (EEP) as well as unequal error protection (UEP) [9] [2]. The latter exploits the advantage of asymmetric power harvesting in a 4-QAM constellation caused by backscatter modulation. Viewed as two independent binary modulations, different levels of protection are offered to the symbol states of a 4-QAM symbol, so as to achieve equal BER post error correction. In Sec. VI, we compare the different modulations and codes using a hypothetical link budget. This provides numerical results to quantify the performance of each scheme.

II. Passive RFID System Model

Passive and semi-passive RFID tags have desirable form factors with a low-power IC connected to external components such as the antenna. The IC integrates several different analog subsystems such as an AC-to-DC voltage converter (power harvester), followed by voltage multiplier and the (data) modulator/demodulator followed by the digital subsections, consisting of a low power microprocessor and a small amount of memory [10] [3]. An impedance matching network placed between the antenna and IC attempts to maximize power transfer from the ambient to on-chip storage element. An early tag implementation was demonstrated by Fischer[11], and present-day industry benchmark is the Monza4 chip from Impinj [12].

During backscatter operation the tag IC is the only active component. The IC modulates the antenna's load impedance, Z_{IC}, via switching a variable impedance component within the tag IC as shown in Fig. 1(a). The mismatch between the antenna's impedance R_{ant} and the IC's impedance Z_{IC} decreases the power transfer from antenna to tag. We next introduce a simple equivalent circuit model to quantify backscatter modulation and power delivered to the tag IC.

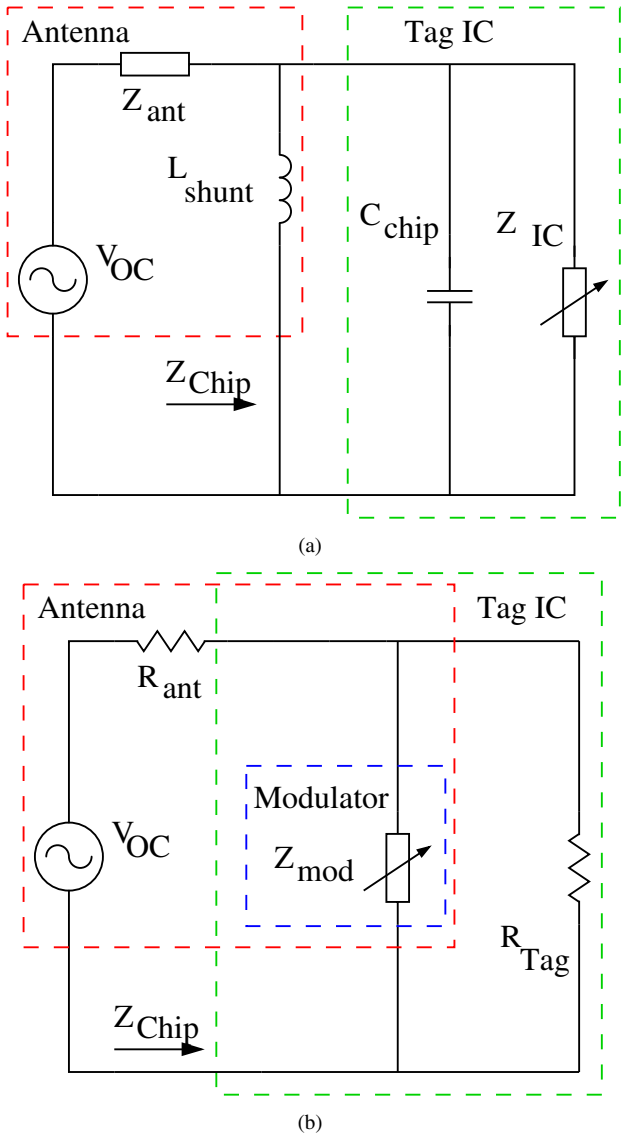

Fig. 1. Tag circuit model before the matching network: (a) illustrates the model antenna inductance and chip capacitance. Whereas (b) has a matching network with the variable components of Z_{IC}, C_{chip}, and L_{shunt} composing Z_{mod}.

A. Equivalent Circuit Model

A Thevenin equivalent model, Fig. 1(a). for the antenna and IC consists of a voltage source V_{OC} with the same frequency as the reader's RF carrier ω, in series with the antenna represented by complex impedance $Z_{ant} = R_{ant} + j\omega L_{ant}$; the tag IC connects to this circuit via a matching network. V_{OC} is the antenna voltage generated by the reader's electric field at the tag. The RFID IC chip impedance is assumed to have a capacitive component in parallel, i.e., $Z_{chip} = Z_{IC} \parallel \frac{1}{j\omega C_{chip}} \parallel j\omega L_{shunt}$, and it is assumed there is a shunt inductance L_{shunt} from the antenna across the tag's IC. The impedance matching network between the chip and antenna

[2]UEP codes protect bits at different levels, whereby both bits are not equally significant in terms of their intrinsic information.

[3]In some designs that target ultra-low power consumption, a finite state machine is used instead of a microprocessor.

is designed such that L_{ant} term cancels at ω of choice, e.g. 915MHz. This leads to a simplified antenna equivalent circuit of R_{ant}[10].

The design of the components assume an operating frequency of 915MHz, however, RFID systems operate within a section of the UHF band, typically $860 - 950$MHz.[4] As the carrier frequency changes, the impedance of frequency dependent components change from their nominal value. Prior work in [8] addresses this issue through RF and device level simulations, and shows negligible performance differences in both BER and EVM due to frequency variations across this range. It leads us to conclude that the equivalent circuit model is a valid abstraction for system analysis.

Define Z_{IC} to be composed of three subcomponents C_{mod}, R_{mod}, and R_{Tag} in parallel. R_{Tag} models the input impedance of all tag IC components other than the modulator circuit, such as digital baseband, demodulator, memory, and power conversion circuits. C_{mod} and R_{mod} are both variable components that make up part of Z_{mod}. Thus the power delivered to R_{Tag} is the power available for use on the tag. The value of R_{Tag} is chosen to equal R_{ant} so that during non-backscatter, the maximum amount of energy transfered from the antenna to the tag is given by

$$P_{match} = \frac{|V_{OC}|^2}{8R_{ant}} \tag{2}$$

Any power delivered to R_{mod} cannot be utilized by the IC and is considered as wasted.

B. Choosing Z_{mod}

A variable Z_{mod} consists of a variable capacitor (bank of varactors), chip capacitance, variable resistor (switched), and a shunt inductor in parallel. Variable components are controlled by the on-tag logic, which can be either a micro-controller or a hardwired state machine. Each set of resistive and capacitive values map to a specific Z_{mod} value, given by

$$Z_{mod} = R_{mod} \parallel j\omega L_{shunt} \parallel \frac{1}{j\omega(C_{mod} + C_{chip})} \tag{3}$$

The mean value of C_{mod} is chosen such that $C_{mean} + C_{chip}$ cancel out L_{shunt} at the frequency of operation, ω_c, i.e.,

$$C_{mean} = \frac{1}{\omega_c^2 L_{shunt}} - C_{chip} \tag{4}$$

This choice of C_{mean} tunes out C_{chip} and L_{shunt}, resulting in $L_{shunt} \parallel (C_{mean} + C_{chip}) = j\infty$; capacitance values greater (less) than C_{mod} generate positive (negative) reactances, respectively.

In general, the combination of L_{shunt} and $C_{mod}+C_{chip}$ is a purely reactive component jX_{mod}. The combined impedance of the circuit is then

$$\begin{aligned} Z_{mod} &= \frac{jR_{mod}X_{mod}}{R_{mod} + jX_{mod}} \\ &= \frac{jR_{mod}X_{mod}}{R_{mod} + jX_{mod}} \frac{R_{mod} - jX_{mod}}{R_{mod} - jX_{mod}} \\ &= \frac{R_{mod}X_{mod}^2 + jR_{mod}^2X_{mod}}{R_{mod}^2 + X_{mod}^2} \end{aligned} \tag{5}$$

[4]The USA uses the 915MHz ISM band, and the EU uses $865-868$MHz.

For any target Z_{mod}, the corresponding R_{mod} and X_{mod} values are then mapped to a circuit level design. Effectively, Z_{mod} behaves a variable impedance with positive and negative reactance and resistance.

C. Backscatter Modulation

During backscatter operation the reader transmits a constant carrier wave that illuminates the tag's antenna with an electromagnetic (EM) field. Corresponding to the physical properties and impedance loading of the tag, a portion of the impinging EM wave is backscattered from the tag. The backscattered wave comprises of two components: a) structural mode and b) antenna mode scattering. Structural mode scattering depends on the physical properties of the antenna, and antenna mode scattering depends on the antenna's impedance load. The physical configuration of the antenna remains independent of any impedance load placed on the antenna [13]. It has been shown by [5] that the net electric field scattered from a tag is

$$\vec{\mathcal{E}}_{scat}^{i} = \vec{\mathcal{E}}_{struct} - \Gamma_i \; I_{match} \; \vec{K}_a \tag{6}$$

where

- $\Gamma_i = \frac{Z_{IC} - R_{ant}}{Z_{IC} + R_{ant}}$ is the reflection coefficient for the i-th modulator state;
- $\vec{\mathcal{E}}_{struct}$ is the structural scattering term;
- $I_{match} = \frac{V_{OC}}{2R_{ant}}$ is the current through R_{ant} when the impedance of the chip and antenna are conjugate matched;
- $\vec{K}_a$ is the Volts per meter per Ampere; the electric field strength radiated by the antenna per unit Ampere of antenna current.

In (6), Γ_i is the only term the tag can modulate with its impedance; the remaining terms are effectively constants. Furthermore, the work of [5] proves that the effect of structural scattering equates to adding a constant offset to a modulated signal. A common approach by the literature assumes $\vec{\mathcal{E}}_{struct} = I_{match} \; \vec{K}_a$ [3] [5], thereby making $\vec{\mathcal{E}}_{scat} \propto I_{ant}$; I_{ant} as the current through the antenna.

For the subsequent discussion, we assume an additive white gaussian noise (AWGN) model and perfect knowledge at the receiver of the constant offset, phase rotation, and symbol synchronization. [5] The net received signal at the reader $y \in \mathbb{C}$ is the sum of three components: a) the modulated antenna mode scattering x_i, b) L as the constant offset from transmit to receive leakage and structual scattering and c) WGN, i.e.,

$$y_i = h \; x_i + L + w \tag{7}$$

where $w \sim \mathcal{CN}(0, N_0)$ and h is a random phase rotation.

Consider a 2-QAM baseband constellation with symbols $x_0 \; , \; x_1 \in \mathbb{C}$ observed by the readers receiver, as modeled by (7). Illustrated by Fig. 2, the constellation has a Euclidean distance of $d = |x_1 - x_0|$ yielding an energy per symbol $E = \left(\frac{|x_1 - x_0|}{2}\right)^2$. Hence, the corresponding bit error probability over an equivalent lowpass AWGN channel with noise

[5]In practice, this is done through parameter estimation on a known preamble sequence.

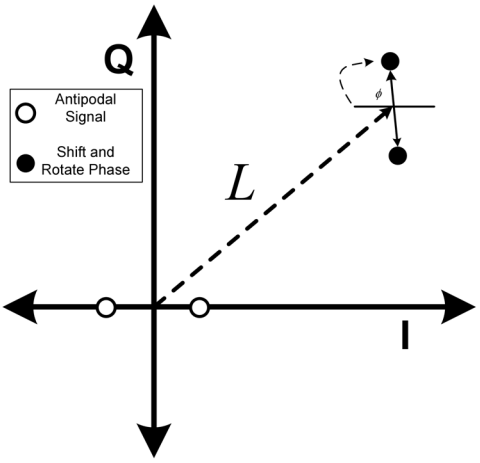

Fig. 2. A binary antipodal constellation where $x_i = \pm 1$, L is a constant offset and $h = e^{-j\phi}$.

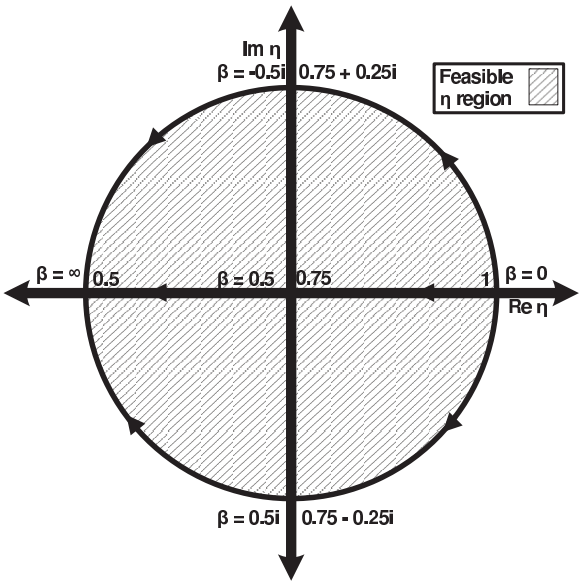

Fig. 3. Visualization of β and $\eta \in W$, (13).

power spectral density of $\frac{N_0}{2}$ is [6]

$$p(e) = Q\left(\sqrt{\frac{2E}{N_0}}\right) \tag{8}$$

We emphasize that in error analysis of digital communication methods such as the above, it is convenient to shift the constellation by an offset equal to the structural mode scattering and transmitter leakage, so as to center them around the origin, since it has no impact on the resulting error probability.

To relate the value of (8) to a set of modulator impedances, consider that $|x_1 - x_0| \propto |\vec{\mathcal{E}}^1_{scat} - \vec{\mathcal{E}}^0_{scat}|$, and $|\vec{\mathcal{E}}^1_{scat} - \vec{\mathcal{E}}^0_{scat}| \propto |I^1_{ant} - I^0_{ant}|$. Thus choosing different I_{ant} via tag impedance modulation is sufficient to design a backscatter constellation. Under the model described by Fig. 1(b), the tag antenna current is given by

$$\begin{aligned} I_{ant} &= \frac{V_{OC}}{Z_{total}} = \frac{V_{OC}}{R_{ant} + Z_{IC}} \\ &= \frac{V_{OC}}{R_{ant} + \frac{R_{Tag} Z_{mod}}{R_{Tag} + Z_{mod}}} \end{aligned} \tag{9}$$

Substituting $R_{Tag} = R_{ant}$, and replacing $Z_{mod} = \beta R_{ant}$, where $\beta \in \mathbb{C}$ is the variable design factor, yields

$$\begin{aligned} I_{ant} &= \frac{V_{OC}}{R_{ant} + \frac{R_{ant} Z_{mod}}{R_{ant} + Z_{mod}}} \\ &= \frac{V_{OC}(R_{ant} + Z_{mod})}{R_{ant}(R_{ant} + Z_{mod}) + R_{ant} Z_{mod}} \\ &= \frac{V_{OC}}{R_{ant}} \left(\frac{1+\beta}{1+2\beta}\right) \end{aligned} \tag{10}$$

Denoting backscatter coefficient

$$\eta_i = \frac{1+\beta_i}{1+2\beta_i} \tag{11}$$

[6]Where $Q(x) = 1 - \Phi(x)$ and $\Phi(x)$ is the CDF of the standard normal distribution.

where i is the modulator state index, we get

$$I_{ant,i} = \frac{V_{OC}}{R_{ant}} \eta_i \tag{12}$$

The relation of the tag antenna current and its induced voltage observed by the reader is further discussed in appendix A.

Clearly, the choice of backscatter symbols η_i determines the BER. Any choice of $\eta \in \mathbb{C}$ is not feasible, because it must map to a valid modulator impedance. A modulator impedance is realizable if the resistive component is non-negative, i.e., $\mathrm{Re}(\beta) \geq 0$. Since

$$\beta = \frac{1-\eta}{2\eta - 1} \tag{13}$$

this implies

$$\mathrm{Re}\left(\frac{1-\eta}{2\eta-1}\right) \geq 0 \tag{14}$$

Simplifying, this yields the feasible set for η:

$$W = \{\eta : \ |\eta - 0.75| \leq 0.25\} \tag{15}$$

Fig. 3 illustrates the region of feasible backscatter symbols in relation to modulator impedance.

Hence, in general the design of a backscatter constellation consists of the following steps.

1) Find a set of $\eta_i \in W$ such the constellation geometry achieves the specified bit error rate vs. tag-reader separation distance and possesses other desirable properties such as symmetry;
2) From (13), solve for β_i, and determine the corresponding impedance values for circuit level design via (5).

III. 4-QAM Constellation Design

It is well-known from communication theory that increasing the number of constellation points improves the bit rate but also requires an increase in SNR (or equivalently, nearest neighbor symbol separation) at the receiver to preserve BER performance. While [8] was the first to suggest higher order

QAM constellations for RFID uplink, we investigate further the issue of achievable QAM constellations from the perspective of power loss due to the coupling of uplink BER performance and power harvesting by the tag. The dependence warrants a new joint design optimization approach, where we describe the preliminaries in this section and formalize in the following section. We investigate a 4-QAM modulation scheme consisting of two independent antipodal encodings on the orthogonal (I) and quadrature (Q) components, respectively, as a case study.

A. Constellation Geometry and Bit Mapping

4-QAM encodes two bits - labeled as the pair (A, B) onto a constellation symbol. We represent a general 4-QAM constellation as four symbols on a circle of radius r centered at $y \in \mathbb{C}$, i.e.,

$$\eta_i = re^{j(\theta_i - \psi)} + y \quad \text{such that } \eta_i \in W, i \in \{0, 1, 2, 3\} \quad (16)$$

where θ_i and r are considered fixed and ψ represents a rotation for *all* symbols. By imposing symmetry, the symbol points are related to each other by

$$\begin{aligned} \theta_0 + \pi &= \theta_2 \\ \theta_1 + \pi &= \theta_3 \end{aligned} \quad (17)$$

From the geometry of a circle, the following is true

$$\begin{aligned} |\eta_0 - \eta_3| &= |\eta_1 - \eta_2| \\ |\eta_0 - \eta_1| &= |\eta_2 - \eta_3| \end{aligned} \quad (18)$$

Assume Gray code labeling, as per Fig. 4. At the reader post demodulation, the constellation points are assumed to be at $\{(\sqrt{E_B}, \sqrt{E_A}), (-\sqrt{E_B}, \sqrt{E_A}), (\sqrt{E_B}, -\sqrt{E_A}), (-\sqrt{E_B}, -\sqrt{E_A})\}$ where

$$\begin{aligned} E_A &\propto |\eta_0 - \eta_3|^2 = |\eta_1 - \eta_2|^2 \\ E_B &\propto |\eta_0 - \eta_1|^2 = |\eta_2 - \eta_3|^2 \end{aligned} \quad (19)$$

The values of E_A and E_B directly map to the parameters r and θ_i.

The BER analysis follows that for quadrature phase shift keying (QPSK), where it is assumed that the AWGN in the I and Q components are independent and identically distributed. The maximum likelihood (ML) decision rule chooses the constellation point nearest to the received signal. It is straight forward to show that the optimal rule for decoding bit A and bit B depends only on $\mathrm{Im}(y_i)$ and $\mathrm{Re}(y_i)$, respectively, where y_i represents the complex sample post demodulation from (7). The corresponding probability of error can be written in terms of the respective symbol energy, E_A and E_B

$$\begin{aligned} p_A(e) &= Q\left(\sqrt{\frac{2E_A}{N_0}}\right) \\ p_B(e) &= Q\left(\sqrt{\frac{2E_B}{N_0}}\right) \end{aligned} \quad (20)$$

Fig. 4 illustrates a realization of bit mapping for two cases: $E_A = E_B$ and $E_A > E_B$.

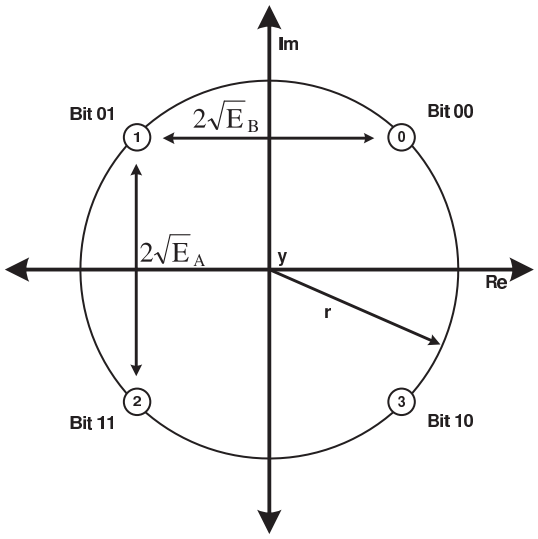

(a) 4-QAM constellation with $E_A = E_B$

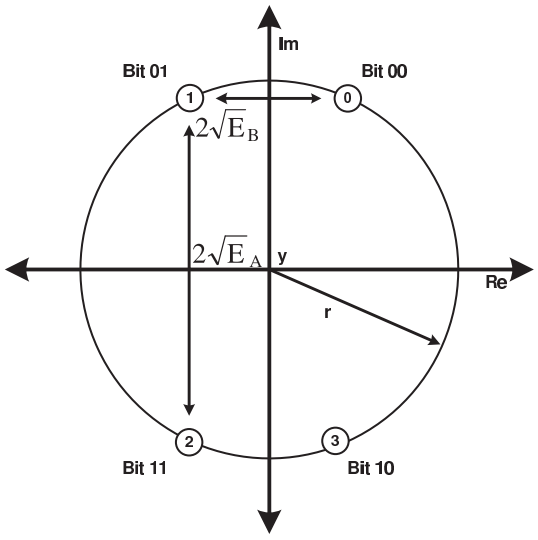

(b) 4-QAM constellation with $E_A > E_B$

Fig. 4. Example 4-QAM constellations described by (16) and (17).

B. Tag Power and Backscatter Modulation

During backscatter, the tag changes its IC impedance Z_{mod} to mismatched state, thereby lowering the power transfer from the antenna (P_{Tag}). Energy lost due to the impedance mismatch is captured by the effective cost, defined as the ratio of energy lost to maximum harvested energy: $\frac{P_{match} - P_{Tag}}{P_{match}}$. The power transfer between a source and a load is maximized if the source and load impedances are conjugate matched, i.e.,

$$Z_{source} = Z_{load}^* \quad (21)$$

Under the equivalent circuit model in Fig. 1(b), the conjugate impedance match condition is met if and only if

$$Z_{IC} = R_{Tag} = R_{ant} \quad (22)$$

The power available to the tag is the power available in R_{Tag}, i.e.,

$$P_{Tag} = \frac{1}{2}|I_{Tag}|^2 R_{Tag} \quad (23)$$

The parallel configuration of Z_{mod} and R_{Tag} is equivalent to a current divider, and hence

$$I_{Tag} = I_{ant}\frac{Z_{mod}}{R_{Tag}+Z_{mod}} = \frac{V_{OC}}{R_{ant}+Z_{IC}}\frac{Z_{mod}}{R_{Tag}+Z_{mod}} \quad (24)$$

Rearranging,

$$\frac{V_{OC}}{R_{ant}+Z_{IC}} = \frac{V_{OC}}{R+\frac{Z_{mod}R_{Tag}}{R_{Tag}+Z_{mod}}} = \frac{V_{OC}(R_{Tag}+Z_{mod})}{R_{ant}(R_{Tag}+Z_{mod})+Z_{mod}R_{Tag}} \quad (25)$$

Substituting back into the (24) and simplifying

$$I_{Tag} = \frac{V_{OC}(R_{Tag}+Z_{mod})}{R_{ant}(R_{Tag}+Z_{mod})+Z_{mod}R_{Tag}}\frac{Z_{mod}}{R_{Tag}+Z_{mod}} = \frac{V_{OC}Z_{mod}}{R_{ant}(R_{Tag}+Z_{mod})+Z_{mod}R_{Tag}} \quad (26)$$

Set $R_{Tag} = R_{ant}$ and $Z_{mod} = \beta R_{ant}$

$$I_{Tag} = V_{OC}\frac{\beta R_{ant}}{R_{ant}^2+2\beta R_{ant}^2} = \frac{V_{OC}}{R_{ant}}\frac{\beta}{1+2\beta} \quad (27)$$

Finally, the power transferred to the tag IC as a function of β

$$P_{Tag}(\beta) = \frac{|V_{OC}|^2}{2R_{ant}}\frac{|\beta|^2}{|1+2\beta|^2} = 4P_{match}\frac{|\beta|^2}{|1+2\beta|^2} \quad (28)$$

Substituting for β in terms of η yields

$$P_{Tag} = P_{Tag}\left(\frac{1-\eta}{2\eta-1}\right) = 4P_{match}\left|\frac{\frac{1-\eta}{2\eta-1}}{1+2\frac{1-\eta}{2\eta-1}}\right|^2 = 4P_{match}\left|\frac{\frac{1-\eta}{2\eta-1}}{\frac{2\eta-1}{2\eta-1}+2\frac{1-\eta}{2\eta-1}}\right|^2 = 4P_{match}\left|\frac{\frac{1-\eta}{2\eta-1}}{\frac{1}{2\eta-1}}\right|^2 = 4P_{match}|1-\eta|^2 \quad (29)$$

Fig. 5 plots the ratio $\frac{P_{Tag}}{P_{match}}$ as a function of $\eta \in \mathbb{C}$. η values near the feasible region boundary, such as 0.5 (impedance match condition), tend to maximize the power transfer. Intuitively, symbols should be placed as close as possible to the P_{match} ($\eta = 0.5$) state in order to maximize average power transfer. Next, we propose an optimization approach for the choice of η_i for a specific constellation such that power transfer is maximized.

IV. Power Loss Minimization

Minimizing P_{loss} (1) is equivalent to maximizing P_{avg}, which is the mean P_{Tag} over the modulator states $\{\eta_0, \eta_1, \eta_2, \eta_3\}$ [7],i.e.,

$$P_{avg}(\eta_0,\eta_1,\eta_2,\eta_3) = \frac{1}{4}\left(P_{Tag}(\eta_0)+P_{Tag}(\eta_1)+P_{Tag}(\eta_2)+P_{Tag}(\eta_3)\right) = P_{match}\left(|1-\eta_0|^2+|1-\eta_1|^2+|1-\eta_2|^2+|1-\eta_3|^2\right) \quad (30)$$

[7]We assume that the symbols are equiprobable.

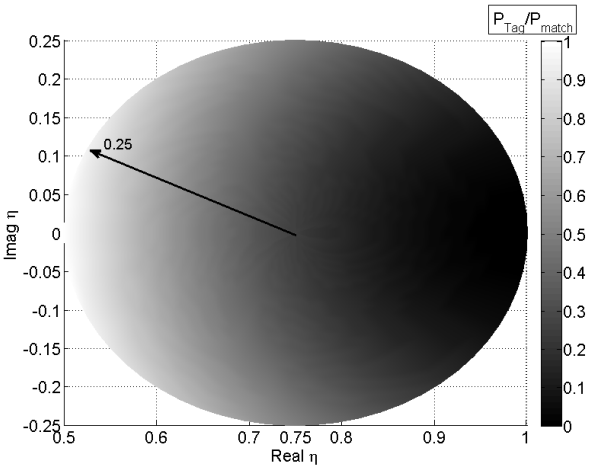

Fig. 5. Graphical visualization of $\eta \in \mathbb{C}$ versus $\frac{P_{Tag}}{P_{match}}$ in gray scale, (29).

We seek the set $\{\eta_i\}$ such that P_{avg} is maximized subject to the following constraints:

- the achievable BER is no greater than a predetermined threshold value, representing reliable link layer operation;
- the set $\{\eta_i\}$ satisfy the geometry described by (16) and (17);
- the set $\{\eta_i\}$ map to feasible modulator impedances (15).

The reliable link requirement determines the parameters $\{r, \theta_i\}$ of (16) to values defined as $\{\hat{r}, \hat{\theta}_i\}$. In this section, we solve for the remaining parameters $\{y, \psi\}$ such that P_{avg} is maximized subject to the constraints described above.

Substituting for η_i in terms of $\{\hat{r}, \hat{\theta}_i, y, \psi\}$, the objective function P_{avg} further simplifies due to the symmetry of 4-QAM; $P_{avg} = P_{match}(\sum_{i=0}^{3}|1-\hat{r}e^{j(\hat{\theta}_0-\psi)}-y|^2)$. From (17), the points η_0 and η_2 satisfy $\hat{r}e^{j(\hat{\theta}_2-\psi)}+y = -\hat{r}e^{j(\hat{\theta}_0-\psi)}+y$; likewise for η_1, η_3. Now, each term in P_{avg} can be written as

$$|1-\hat{r}e^{j(\hat{\theta}_i-\psi)}-y|^2 = |1-y|^2 - 2\mathrm{Re}\{(1-y^*)\hat{r}e^{j(\hat{\theta}_i-\psi)}\}+\hat{r}^2 \quad (31)$$

Using the fact that $\hat{r}e^{j(\hat{\theta}_2-\psi)} = -\hat{r}e^{j(\hat{\theta}_0-\psi)}$, cancels out the $\mathrm{Re}\{.\}$ terms, leading to

$$|1-\hat{r}e^{j(\hat{\theta}_0-\psi)}-y|^2+|1-\hat{r}e^{j(\hat{\theta}_2-\psi)}-y|^2 = 2(|1-y|^2+\hat{r}^2) \quad (32)$$

and resulting in

$$P_{avg} = 4P_{match}(|1-y|^2+\hat{r}^2) \quad (33)$$

Hence ignoring scalar multiplier and additive constants, the optimization problem seeks to

$$\text{Maximize}_{y,\psi}\ \ |1-y|^2 \quad (34)$$
$$\text{Subject to: } |\hat{r}e^{j(\hat{\theta}_i-\psi)}+y-0.75| \le 0.25\ ,\ 0 \le i \le 3$$
$$0 \le \psi \le 2\pi\ ,\ y \in \mathbb{C}$$

The first set of constraints ensure that the η_i found by the optimization are feasible (15). Geometrically interpreted, the η_i correspond to four corners of a rectangle centered at y, which is confined to the region of feasible η_i; see Fig 6. The choice of ψ rotates the constellation points around the center y.

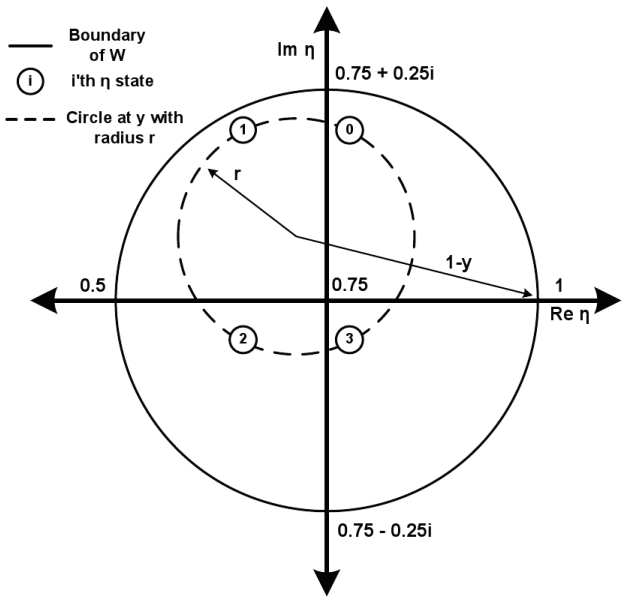

Fig. 6. To maximize P_{avg} choose y and ψ (rotation of the η_i points) such that $|1-y|$ is maximized, and η_i remain confined to W (15).

To solve for the optimal $\{y, \psi\}$, we exhaustively search over all possible $\{y, \psi\}$ as follows. We first collect a list of y values that satisfy the constraints of (34) for some choice of ψ. From this list, we choose the y that maximizes $|1-y|^2$. Appendix C offers an alternative geometric interpretation for the optimal $\{y, \psi\}$.

Fig. 7(a) illustrates an example of two 4-QAM constellations (optimal and sub-optimal) where the values for E_A and E_B are chosen arbitrarily. The normalized average power loss $\frac{P_{avg}-P_{match}}{P_{match}} = 0.27$ for the optimized case and $\frac{P_{match}-P_{avg}}{P_{match}} = 0.84$ for the non-optimized example. Fig. 7(b) plots the set of all feasible y vs $|1-y|^2$, which shows that the optimal y occurs at the point closest to the matched state. However the optimal η_i does not include the matched state (which maximizes P_{Tag} for that state) as one of the modulator states.

V. Coded Modulation Design

Increasing the modulation order improves spectral efficiency but decreases the power harvested P_{avg}. To fairly compare different modulations and FEC codes, we use the normalized power loss per bit (1)

$$P_{loss} = \frac{P_{match} - P_{avg}}{C\, P_{match}}$$

Backscatter, when there is an impedance mismatch between the tag and antenna, results in a power penalty to the tag. Hence for a symbol period T_s, the average energy lost per symbol due to mismatch is $T_s(P_{match} - P_{avg})$; if no backscatter occurs, the energy harvested per symbol period is $T_s P_{match}$. Normalizing the energy lost with respect to the maximum energy harvested per symbol gives $\frac{P_{match}-P_{avg}}{P_{match}}$, the average fraction lost per symbol. To account for different spectral efficiency (C), we use the percentage of power lost per bit or normalized power loss per bit. This section explores the use of FEC coding to improve (lower) P_{loss} required for 4-QAM as compared to the uncoded case.

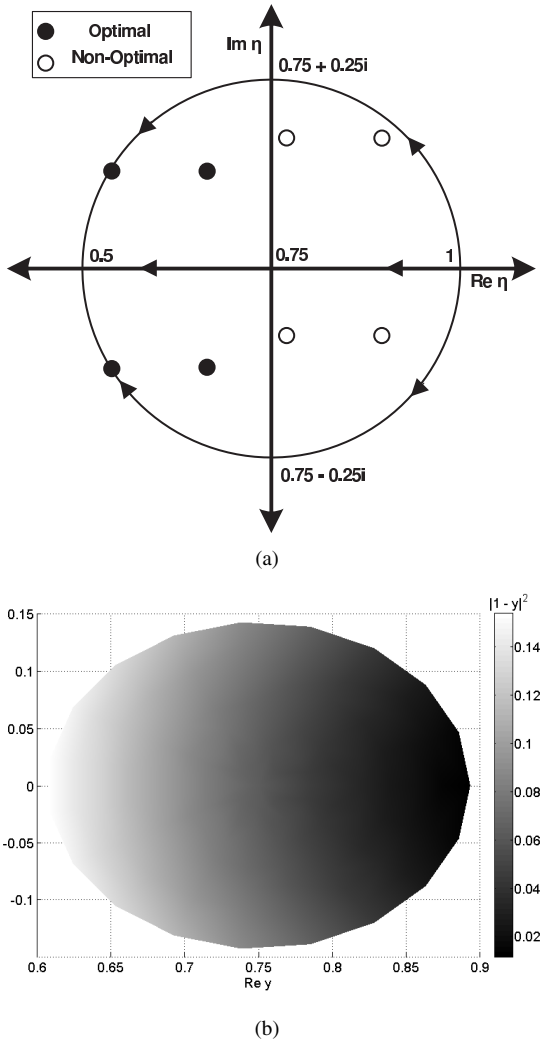

Fig. 7. Figure (a) Example of backscatter symbol placement for a 4-QAM constellation geometry ($r = 0.15$,$\theta_0 = \frac{4\pi}{11}$,$\theta_1 = \frac{7\pi}{11}$,$\psi = 0$): optimal and non-optimal. Figure (b) plots y (16) vs. $|1-y|^2$ for the same constellation parameters as (a).

Additionally, we emphasize that lower P_{loss} only implies improved power harvesting during backscatter. So for a typical passive RFID tag reading scenario, where a tag spends most of its time idle and only transmits a short EPC, an improved P_{loss} has a smaller impact as opposed to a sensor network application. A sensor network moves a larger volume of information from each sensor, thereby increasing the system impact on the cost to send each bit.

A. Uncoded 2-QAM and 4-QAM Modulation

The uncoded 2-QAM constellation follows directly from the modulations described in the Gen2 standard [6]. Two common binary modulator designs in current use - (binary) ASK and PSK - achieve the same BER given by (8). However, ASK uses only resistive modulator impedances while PSK uses only reactive modulator impedances. Even though both have

identical link performance, PSK achieves a lower P_{loss} than ASK.

The 4-QAM constellation is designed by the method discussed in Sec. III-B. Both bits have equal probability of error, which leads to a constellation with equal distance between symbols as illustrated by Fig. 4(a) ($E_A = E_B$) and BER given by (20).

B. Coded 4-QAM: UEP and EEP

The proposed 4-QAM constellation along with a suitable forward error correction code promises new options to balance desired uplink rates and power harvesting. The coding gain allows for reliable bit decoding at a lower SNR, allowing for a new modulator design with different impedances. Lower SNR requirements maps to constellations with higher P_{avg}, which could be used for a variety of purposes - e.g. increased uplink range or improved link reliability or support operation of additional sensing circuits. But FEC codes also decrease the amount of info. bits per symbol (C). Thus it is necessary to examine both P_{avg} and code choice.

The performance of FEC options with memory - such as convolutional coding - provides appropriate guidelines for the choice of coding to be used in conjunction with 4-QAM. Recall that our choice of 4-QAM constellation is equivalent to two orthogonal BPSK signals. The probability of bit error $p_b(e)$ of a coded BPSK signal at high SNR has a good approximation[14], and the corresponding BER for bit A and B is

$$p_A(e) \approx Q\left(\sqrt{\frac{2E_{b,A}Rd_{free}}{N_0}}\right) \tag{35}$$

$$p_B(e) \approx Q\left(\sqrt{\frac{2E_{b,B}Rd_{free}}{N_0}}\right) \tag{36}$$

where R is the code rate, d_{free} is the free distance of the code, and ($E_{b,A}\, E_{b,B}$) is the respective energy per information bit. This approximation to the BER is used to calculate the reader's BER for the UEP and EEP schemes.

In the case of EEP, the total symbol energy is distributed equally to both bits that are coded with identical FEC, resulting in equal error protection: $p_A(e) = p_B(e)$. Additionally, the FEC can decode bits with the same reliability as uncoded detection using a factor of d_{free} less energy per symbol, or Rd_{free} less energy per bit. Lowering the symbol energy maps to decreasing r of the constellation (16) Constellations with smaller r and constant θ_i result in backscatter modulator designs with a higher P_{avg}. The P_{avg} is calculated using two different FECs, each with different rates and d_{free}, specifically ($R = \frac{1}{2}$, $d_{free} = 8$), and ($R = \frac{3}{4}$, $d_{free} = 5$). The inclusion of the new P_{avg} and the new info. rate (because of FEC) results in the new P_{loss}.

The second approach uses a variation of UEP coding. Originally, the motivation for UEP was to design codes that provide unequal protection for each bit based on the differences in their respective significance [15]. However, in our work, we use UEP FEC to yield equal bit error rates post coding for a constellation with unequal BER when uncoded, i.e., for the 4-QAM case where $p_A(e) \neq p_B(e)$. From (20), unequal error probabilities requires asymmetry in the constellation as illustrated by Fig. 4(b) which is then compensated by the UEP FEC.

In case of an asymmetry between the reactive (quadrature) and resistive (inphase) bits, PSK out performs ASK modulation in terms of power harvesting[4]. To minimize the power loss of the resistive modulated (B) bit, the symbol energy for bit B is decreased (by an amount determined by the FEC coding gain), i.e. $E_B < E_A$ as in Fig. 4(b). Decreasing only E_B and keeping E_A constant thereby decreases the constellation's r and changes θ_0 and θ_1. These changes in constellation geometry allow for a feasible backscatter modulator with a higher P_{avg}. To maintain reliability, this bit is then protected with a FEC. Bit A is otherwise left *uncoded*, which results in $1 + R$ information bits per symbol. Leaving a bit uncoded also reduces complexity at the reader, because only part of the constellation is required to be processed by the FEC decoder. Lastly, the same two codes used in EEP are used to encode bit B and in addition a code with $R = \frac{1}{4}$ and $d_{free} = 18$ is also used.

VI. Numerical Results

Table VI displays the normalized power lost per information bit $\frac{P_{match} - P_{avg}}{C\, P_{match}}$ for each of the modulations discussed previously. Each combination of constellation and FEC is designed to meet an uplink range of 25 m, a BER of 10^{-3} and 10^{-5}, for a fixed symbol rate of 640 KHz. The SNR and P_{avg} is calculated using the approach discussed in Sec. II-C and Sec. III-B. Additionally, the values for the reader and tag parameters are listed in Appendix B. As expected, PSK has the superior power loss figure as compared to ASK, despite the fact that at the receiver, the two constellations are identical in BER and information rate. The next notable result is the difference in performance between uncoded 4-QAM and PSK. As discussed in Sec. III-A, the uncoded 4-QAM constellation is equivalent to a mean shifted QPSK constellation. From communication theory, it is well-known that BPSK and QPSK have identical power cost per bit. However in this example, the 4-QAM constellation is considerably more expensive in terms of the normalized power loss than PSK.

UEP performs the best out of all the code choices, except for 2-PSK. Despite UEP and EEP using identical FECs, UEP performs better. For nearly equal P_{loss}, EEP achieves better spectral efficiency at the same reliability. Indicating that the majority of the power is lost in the resistive modulated bit as opposed to reactive modulated bit. Hence in this example, coding the reactive bit (A) is less efficient than leaving the bit uncoded. Additionally, it explains that constellation design for backscatter modulation should be treated differently than traditional modulation by including the notion of (normalized) power cost, which is not bit-wise identical. Finally, it demonstrates the importance of co-design of the constellation and FEC.

While 2-PSK out performs UEP in terms of normalized power cost, UEP offers better spectral efficiency than PSK. UEP also outperforms uncoded 4-QAM for both BER constraints. This suggests that a system designer should consider UEP coding in conjunction with 4-QAM for RFID uplink, if that is a feasible option given the overall specifications.

TABLE I
NORMALIZED POWER LOSS PER INFORMATION BIT FOR DIFFERENT MODULATIONS AND FECS. THE NUMERICAL RESULT IS CALCULATED FROM A HYPOTHETICAL TAG AND READER SETUP

Modulation Type	P_{loss} at $p(e) = 10^{-3}$	P_{loss} at $p(e) = 10^{-5}$	C
2-PSK	0.001	0.003	1
UEP $R = 1/4$ $d_{free} = 18$	0.017	0.024	1.25
UEP $R = 1/2$ $d_{free} = 8$	0.021	0.029	1.5
UEP $R = 3/4$ $d_{free} = 5$	0.022	0.031	1.75
EEP $R = 3/4$ $d_{free} = 5$	0.025	0.034	1.5
EEP $R = 1/2$ $d_{free} = 8$	0.03	0.041	1
4-QAM	0.04	0.057	2
2-ASK	0.08	0.11	1

VII. CONCLUDING REMARKS

This work provided a new analysis for RFID link that integrates the traditional communication metrics (BER and spectral efficiency) with the notion of (normalized) power loss per bit. The latter is an important consideration in power starved RFID tags that must rely on harvested power for operation. Its inclusion couples the downlink with the uplink via the choice of the power harvesting circuitry parameters (downlink) and (uplink) constellation design - this distinguishes our work from traditional communications.

Our results show a significant increase in the normalized power loss from 2-QAM to 4-QAM in return for the increased spectral efficiency of the latter. Consequently, we propose novel coded 4-QAM schemes based on UEP that help bridge the gap in performance between 2-QAM and 4-QAM. These new PHY layer options may provide guidance for future Class 1 Gen 2 enhancements that yield a better balance between the tag's two key attributes: harvested energy and uplink efficiency.

APPENDIX A
RF BACKSCATTER MODEL

To relate the physical properties of the tag and reader during backscatter, we briefly restate the key developments from [3]. The electric field at the tag $\mathcal{E}_{Tag}$ depends on the reader's effective isotropic radiated power (EIRP) P_{EIRP}, the distance between the tag and reader l, and the polarization match coefficient ρ. P_{EIRP} is related by the raw transmit power P_{rdr} and reader antenna gain G_{rdr}: $P_{rdr}G_{rdr} = P_{EIRP}$

$$\mathcal{E}_{Tag} = \sqrt{\frac{Z_0 \rho P_{EIRP}}{4\pi l^2}} \tag{37}$$

where Z_0 is free-space impedance. The open circuit voltage V_{OC} is proportional to the $\mathcal{E}_{Tag}$ and given by

$$V_{OC} = \alpha_{Tag}\mathcal{E}_{Tag} = \alpha_{Tag}\sqrt{\frac{Z_0 \rho P_{EIRP}}{4\pi l^2}} \tag{38}$$

The α_{Tag} variable relates the physical geometry of the antenna to the incident electric field. The electric field generated by the tag's antenna is proportional to current passing through the antenna, I_{ant}. At the reader's antenna, the reflected electric field is

$$\mathcal{E}_{rdr} = I_{ant}\frac{Z_0 \alpha_{Tag}}{2\lambda l} \tag{39}$$

where λ is the wavelength of the carrier wave. $\mathcal{E}_{rdr}$ induces a voltage V_{rdr} across the reader's antenna, which is measured by the receiver to make a bit decision.

$$V_{rdr} = \alpha_{rdr}\mathcal{E}_{rdr} = \alpha_{rdr} I_{ant}\frac{Z_0 \alpha_{Tag}}{2\lambda l} \tag{40}$$

Lastly, the reader's receiver is subject to noise from thermal affects and from phase noise leakage from the transmitter circuit. It is understood in RFID applications that phase noise dominates thermal noise [4]. A typical observed phase noise power is $-115\frac{\text{dBc}}{\text{Hz}}$. We assume there is a power reduction factor of 15dB between the receiver and transmitter circuits, and a further reduction of 50dB for the conversion of phase noise to amplitude noise. ($-115\frac{\text{dBc}}{\text{Hz}} - 15\text{dB} - 50\text{dB} = -180\frac{\text{dBc}}{\text{Hz}}$)

$$N_0 = -180\frac{\text{dBc}}{\text{Hz}} \tag{41}$$

Relating the above parameters to the observed SNR at the reader $\text{SNR} = \frac{E}{N}$ for 2-QAM modulation is achieved by noting that the instantaneous signal power

$$\begin{aligned} E &= \left(\frac{|x_1 - x_0|}{2}\right)^2 \\ &= \left(\frac{1}{2\sqrt{2}}|V_{rdr,0} - V_{rdr,1}|\right)^2 \\ &= \left(\frac{1}{2\sqrt{2}}|I_{ant,0} - I_{ant,1}|\frac{|\alpha_{rdr}||\alpha_{Tag}|Z_0}{2\lambda l}\right)^2 \\ &= \left(\frac{1}{2\sqrt{2}}|\eta_0 - \eta_1|\frac{|V_{OC}|}{R_{ant}}\frac{|\alpha_{rdr}||\alpha_{Tag}|Z_0}{2\lambda l}\right)^2 \\ &= |\eta_0 - \eta_1|^2\left[\frac{1}{2\sqrt{2}}\frac{1}{R_{ant}}|\alpha_{Tag}|\sqrt{\frac{Z_0 \rho P_{EIRP}}{4\pi l^2}}\right]^2 \\ &\quad \left[\frac{|\alpha_{rdr}||\alpha_{Tag}|Z_0}{2\lambda l}\right]^2 \end{aligned} \tag{42}$$

and noise power

$$N = P_{rdr} B N_0 \tag{43}$$

This equation for SNR can be used to calculate the uplink BER by (8) the antipodal signaling BER.

APPENDIX B
VALUES FOR RFID SYSTEM PARAMETERS

The system parameter values discussed and defined in Appendix A are listed here:

$$\begin{array}{ccc} P_{rdr} = 1\text{W} & G_{rdr} = 6\text{dB} & B = 640\text{KHz} \\ |\alpha_{Tag}| = 0.1 & |\alpha_{rdr}| = 0.12 & \lambda = 0.32\text{m} \\ l = 25\text{m} & Z_0 = 377\Omega & \rho = 0.5 \\ R_{ant} = 76\Omega & & \end{array}$$

APPENDIX C
GEOMETRIC INTERPRETATION OF P_{loss} MINIMIZATION

Section IV presented a numerical approach to solving the optimization problem posed by (34). In the following we argue optimality of the constellation geometry shown in Fig 7(a) for any choice of $\{\hat{r}, \hat{\theta}_i\}$ via a geometric proof; sketched as the following:

- the optimal solution occurs when at least two symbols, η_i, lay on the boundary of W (15);
- the set of feasible y can be reduced to $|y - 0.75| \leq d$ where d depends on E_A and E_B;
- for a constellation with $E_A > E_B$, $y^\star = 0.75 - \sqrt{0.25^2 - E_A} + \sqrt{E_B}$.

As described in Section III the choice of $\{\hat{r}, \hat{\theta}_i\}$ map directly to the values of E_A and E_B. For any fixed ψ, the optimization problem described by (34) is the maximization of a convex function over a closed convex set [16], and convex analysis [17] states that the maximum occurs somewhere on the constraint boundary of W, i.e. at least one constraint is met with equality.

From the rectangular geometry of the four η_i points and the circle shape of constraint region W, the set of all feasible y can be reduced to a circle defined by $|y - 0.75| \leq d$; Fig 7(a) illustrates the relationship between η_i and W. The value of d depends on the lengths of the rectangle's sides, and from Pythagorean equation it can be written as:

$$\{y : \ |y - 0.75| \leq \sqrt{0.25^2 - E_A} - \sqrt{E_B}, \ E_A > E_B\} \quad (44)$$

or

$$\{y : \ |y - 0.75| \leq \sqrt{0.25^2 - E_B} - \sqrt{E_A}, \ E_A \leq E_B\} \quad (45)$$

Therefore the $y^\star$ that maximizes $|1 - y|$ clearly occurs at the boundary of W where

$$y^\star = 0.75 - \sqrt{0.25^2 - E_A} + \sqrt{E_B}, \ E_A > E_B \quad (46)$$

or

$$y^\star = 0.75 - \sqrt{0.25^2 - E_B} + \sqrt{E_A}, \ E_A \leq E_B \quad (47)$$

REFERENCES

[1] D. Yeager, P. Powledge, R. Prasad, D. Wetherall, and J. Smith, "Wirelessly-charged UHF tags for sensor data collection," in *Proc. 2008 IEEE International Conference on RFID*, pp. 320–327.

[2] A. Sample, D. Yeager, P. Powledge, and J. Smith, "Design of a passively-powered, programmable sensing platform for UHF RFID systems," in *Proc. 2007 IEEE International Conference on RFID*, pp. 149–156.

[3] R. Chakraborty, S. Roy, and V. Jandhyala, "Revisiting RFID link budgets for technology scaling: range maximization of RFID tags," *IEEE Trans. Microwave Theory and Techniques*, vol. 59, no. 2, pp. 496–503, 2011.

[4] D. Dobkin, *The RF in RFID*. Elsevier Inc., 2008.

[5] F. Fuschini, C. Piersanti, F. Paolazzi, and G. Falciasecca, "Analytical approach to the backscattering from UHF RFID transponder," *IEEE Antennas and Wireless Propag. Lett.*, vol. 7, pp. 33–35, 2008.

[6] EPC Global, EPC Global RFID Protocol Class 1 Generation 2 UHF, Jan. 2005.

[7] M. Simon and D. Divsalar, "Some interesting observations for certain line codes with application to RFID," *IEEE Trans. Commun.*, vol. 54, pp. 583–586, Apr. 2006.

[8] S. Thomas and M. S. Reynolds, "QAM backscatter for passive UHF RFID tags," in *Proc. 2010 IEEE International Conference on RFID*, pp. 210–214.

[9] B. Masnick and J. Wolf, "On linear unequal error protection codes," *IEEE Trans. Inf. Theory*, vol. 13, pp. 600–607, Oct. 1967.

[10] G. D. Vita and G. Iannacone, "Design criteria for the RF section of UHF and microwave passive RFID transponders," *IEEE Trans. Microwave Theory and Techniques*, vol. 53, pp. 2978–2990, Sep. 2005.

[11] U. Karthaus and M. Fischer, "Fully integrated passive UHF RFID transponder IC with 16.7- μ W minimum RF input power," *IEEE J. Solid-State Circuits*, vol. 38, pp. 1602–1608, Oct. 2003.

[12] Impinj Corp., Monza 4 Tag Chip Datasheet, 2010. Available: http://www.impinj.com/products/monza4tagchips.aspx.

[13] R. Hansen, "Relationships between antennas as scatterers and as radiators," *Proc. IEEE*, vol. 77, pp. 659–662, May 1989.

[14] U. Madhow, *Fundamentals of Digital Communication*. Cambridge, 2008.

[15] R. Morelos-Zaragoza and S. Lin, "QPSK block-modulation codes for unequal error protection," *IEEE Trans. Inf. Theory*, vol. 41, pp. 576–581, Mar. 1995.

[16] S. Boyd and L. Vandenberghe, *Convex Optimization*. Cambridge University Press, 2004.

[17] R. T. Rockafellar, *Convex Analysis*. Princeton University Press, 1997.

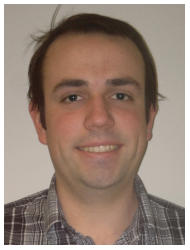

Colby Boyer Colby Boyer received the B.S. degree in Electrical Engineering and Computer Science from the University of California Berkeley in 2009. He joined Eta Kappa Nu in 2006 and IEEE as a student member in 2007. Currently he is pursuing a Ph.D. degree in Electrical Engineering at the University of Washington. His current research interests include low power wireless communication and its application to RFID. In the past, he has held summer internships at Los Alamos National Laboratory and Qualcomm Inc.

Sumit Roy Sumit Roy received the B. Tech. degree from the Indian Institute of Technology (Kanpur) in 1983, and the M. S. and Ph. D. degrees from the University of California (Santa Barbara), all in Electrical Engineering in 1985 and 1988 respectively, as well as an M. A. in Statistics and Applied Probability in 1988. Presently, he is Prof. of Electrical Engineering, Univ. of Washington where his research interests include analysis/design of communication systems/networks, with an emphasis on next generation mobile/wireless and sensor networks. He spent 2001-03 on academic leave at Intel Wireless Technology Lab as a Senior Researcher engaged in research and standards development for ultra-wideband systems (Wireless PANs) and next generation high-speed wireless LANs. He served as Science Foundation of Ireland Isaac Walton Fellow during a sabbatical at University College, Dublin (Jan-Jun 2008) and was the recipient of a Royal Acad. Engineering (UK) Distinguished Visiting Fellowship during summer 2011. He was elevated to IEEE Fellow by Communications Society in 2007 for his contributions to multi-user communications theory and cross-layer design of wireless networking standards. He currently serves on the Editorial Board for IEEE TRANSACTIONS ON COMMUNICATIONS, IEEE JOURNAL ON INTELLIGENT TRANSPORTATION SYSTEMS and the IEEE TRANSACTIONS ON SMART GRIDS.